frontiers | Frontiers in Earth Science

TYPE Original Research
PUBLISHED 11 January 2023
DOI 10.3389/feart.2022.1007342

OPEN ACCESS

EDITED BY
Danqing Song,
Tsinghua University, China

REVIEWED BY
Zhuo Chen,
Sichuan Agricultural University, China
Lulu Liu,
China University of Mining and Technology, China
Mengxin Liu,
Northeast Forestry University, China

*CORRESPONDENCE
Zhijian Wu,
zhijian@njtech.edu.cn

SPECIALTY SECTION
This article was submitted to Geohazards and Georisks, a section of the journal Frontiers in Earth Science

RECEIVED 30 July 2022
ACCEPTED 21 October 2022
PUBLISHED 11 January 2023

CITATION
Bi J, Wu Z, Lu Y, Wen H, Zhang Y, Shen Y, Wei T and Wang G (2023), Study on soil freezing characteristic curve during a freezing-thawing process.
Front. Earth Sci. 10:1007342.
doi: 10.3389/feart.2022.1007342

Study on soil freezing characteristic curve during a freezing-thawing process

Jun Bi[1], Zhijian Wu[1]*, Yu Lu[1], Haiyan Wen[2], Yingmin Zhang[3], Yunxia Shen[4], Tingting Wei[1] and Guoxu Wang[1]

[1]College of Transportation Engineering, Nanjing Tech University, Nanjing, China, [2]State Key Laboratory of Seed Innovation and Grassland Agro-ecosystems, College of Pastoral Agriculture Science and Technology, Lanzhou University, Lanzhou, China, [3]CCCC First Harbor Consultants Co., Ltd, Tianjin, China, [4]School of Cultural Heritage, Northwest University, Xi'an, China

Soil freezing characteristic curve (SFCC) defines the relationship between unfrozen water content and subzero temperature. The SFCC is widely applied to estimate the soil properties. The current study explored the effects of initial water content, dry density, soil type and desalination on the SFCC during a freezing-thawing process. It showed that the initial water content, soil type and desalination had great impacts on SFCC, while the dry density had an insignificant effect on SFCC. Hysteresis behavior was observed for all the soil samples. The hysteresis behavior was obvious in the temperature range of -5°C < T < 0, but not obvious in the temperature range of $T \leq$ -10 °C. A new equation containing freezing/thawing point was proposed to model the SFCC. The new model and four SFCC models were evaluated with measured data in this study. It showed that the new model performed best among these models. The new model accurately mimics the SFCC and is continuous near the freezing/thawing point and 0 °C. It can be easily incorporated into numerical algorithms for coupled heat and mass transfer in cold regions.

KEYWORDS

unfrozen water content, soil freezing characteristic curve, freezing-thawing process, hysteresis behavior, freezing point

1 Introduction

In freezing soils, a small amount of liquid water exists because of the capillarity and surface energy of soil particles (You et al., 2017; Li et al., 2020). The relationship between unfrozen water content and subzero temperature can be termed as soil freezing characteristic curve (SFCC). The SFCC is one of the vital hydromechanical properties of freezing soils and can be applied to estimate hydraulic conductivity (Ming et al., 2022), resilient modulus (Ren and Vanapalli, 2018), and thermal conductivity (Bi et al., 2019; Bi et al., 2020).

Experimental measurement and calculation method can be applied to determine unfrozen water content (Wen et al., 2012). The experimental measurement techniques include pulsed nuclear magnetic resonance method (Watanabe and Wake, 2009), time/frequency domain reflectometry method (Patterson and Smith, 1985; Xiao et al., 2018), calorimetry method (Kozlowski and Nartowska, 2013), and dilatometry method (Konrad, 1994). Experimental

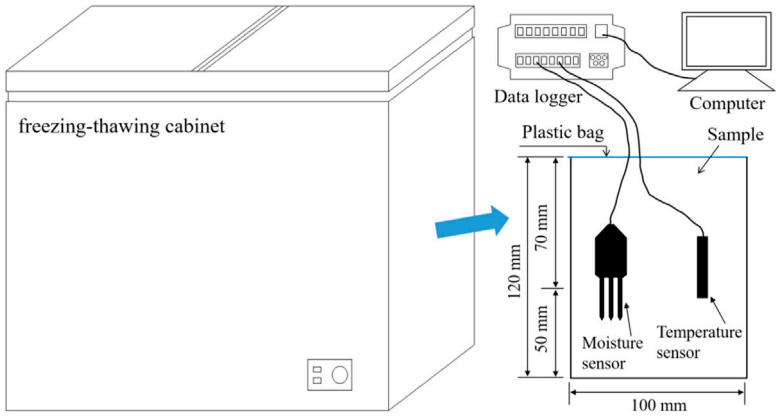

FIGURE 1
Experimental apparatus for freezing-thawing test.

efforts have shown that the SFCC is affected by dry density, water content, confining stress, and salinity (Zhang et al., 2018; Mu et al., 2019; Liu et al., 2020; Xiao et al., 2020). Most researches have investigated the freezing branch of SFCC, but few researches studied the thawing branch of SFCC and hysteresis behavior.

Some unfrozen water content models were developed by the combination of soil water characteristic curve (SWCC) model and Clapeyron equation. For example, Bittelli et al. (2003) developed a SFCC model by using the van Genuchten SWCC model and neglecting the overburden pressure. Nishimura et al. (2009) substituted a Clausius-Clapeyron equation into the van Genuchten SWCC model, and obtained a SFCC model without considering the effect of ice pressure. Ren et al. (2017) revealed the similarity between SWCC and SFCC, and reviewed three SFCC models (Brooks and Corey SFCC model, van Genuchten SFCC model, and Fredlund and Xing SFCC model). These SFCC models have good performance in modeling the relationship between unfrozen water content and subzero temperature. However, these models didn't consider freezing/thawing point. Therefore, the current study develops a new SFCC model containing freezing/thawing point during a freezing-thawing process.

The study aims to 1) analyze the effect of different properties on the SFCC and hysteresis behavior during a freezing-thawing process, 2) propose a new model containing freezing/thawing point to describe the SFCC, and 3) evaluate the new SFCC model and some published SFCC models using the measured data.

2 Materials and methods

2.1 Experimental apparatus

In this study, a freezing-thawing cabinet with a controlled temperature from -30°C to +20°C was used to measure SFCC

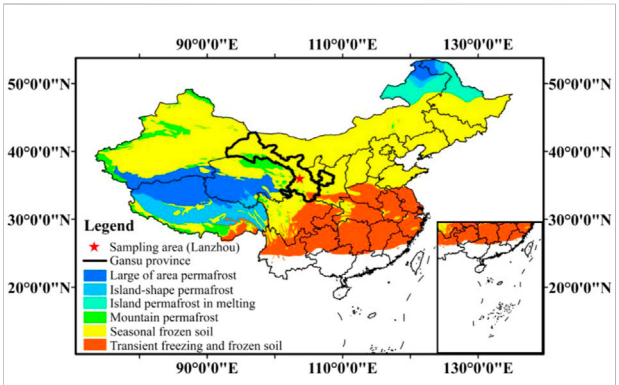

FIGURE 2
Sampling area.

(Figure 1). Each sample was equipped with a moisture sensor and a temperature sensor. The moisture sensor has an accuracy of ±3%, while the temperature sensor has an accuracy of ±0.05°C. All the sensors were put in the middle of the soil sample and connected to a CR6 data logger, with measurements recorded at 30-s intervals.

2.2 Experimental method

The loess was collected from Lanzhou, Gansu Province, as shown in Figure 2. Its liquid and plastic limits are 25.92% and 16.75%, respectively. Table 1 shows properties of six soil samples. S01, S02 and S03 were prepared for investigating the effect of initial water content. S02 and S04 can be used to investigate the effect of dry density. S01 and S05 can be applied to study the effect of soil types. S01 and S06 can be used to investigate the effect of desalination.

TABLE 1 Properties of six soil samples.

NO.	Initial water content (%)	Dry density (g/cm^3)	Loess content (%)	Sand content (%)	Loess
S01	11	1.65	100	0	loess
S02	14	1.65	100	0	loess
S03	17	1.65	100	0	loess
S04	14	1.55	100	0	loess
S05	11	1.65	70	30	loess
S06	11	1.65	100	0	desalted loess

TABLE 2 Freezing/thawing method and controlled temperatures.

Freezing method	Thawing method	Controlled temperatures/°C
Step freezing	Step thawing	0.5, 0, -0.5, -1.0, -1.5, -2.0, -2.5, -3.0, -3.5, -4.0, -4.5, -5.0, -7.0, -10.0, -15.0, -20.5, -15.0, -10.0, -7.0, -5.0, -4.5, -4.0, -3.5, -3.0, -2.5, -2.0, -1.5, -1.0, -0.5, 0, 0.5

For desalted loess, distilled deionized water was used to eliminate salts. Thereafter, the desalted loess, loess and sand were oven-dried at a temperature of 105°C for more than 24 h. The oven-dried loess was filtered by 2-mm sieve to remove the impurity. The mass of the over-dried loess, over-dried sand and distilled deionized water for one sample can be calculated using equations in Appendix A.

For loess samples, the required mass of distilled deionized water and oven-dried loess were evenly mixed to reach the desired water content. To obtain a uniform moisture distribution, the mixture was kept in a sealed plastic bag for 24 h. For loess-sand mixed samples, in order to obtain uniform moisture distribution, they followed the same procedure.

The diameter and height of soil sample were 100 mm and 120 mm, respectively. To achieve a desired dry density, the sample was tamped in 12 layers. A moisture sensor and a temperature sensor were put in the middle of soil sample, as shown in Figure 1. To avoid water evaporation, the plastic bags were applied to cover the top surface of the sample. After that, the soil specimens were kept at 0.5 °C for 24 h to achieve hydro-thermal balance. The experiment was conducted in accordance with the changes of controlled temperatures, as listed in Table 2. At each controlled temperature, the soil specimens were kept for 12 h to reach hydro-thermal balance.

2.3 Models

2.3.1 VG SFCC model

Previous studies have shown that the SFCC model can be derived by combining Clapeyron equation and SWCC model, which can mimic the relationship between unfrozen water content and subzero temperature during a freezing-thawing process (Zhang et al., 2016; Zhang et al., 2018; Wen et al., 2020), as shown in Eq. 1. The procedure for obtaining Eq. 1 was in Appendix B.

$$\theta = \theta_r + (\theta_s - \theta_r)\left[\frac{1}{1+\left(-\frac{\alpha L \rho_w}{273.15}T\right)^n}\right]^m \quad (1)$$

where θ refers to volumetric water content, θ_r refers to residual volumetric water content, θ_s refers to saturated volumetric water content, L refers to latent heat of fusion of water, ρ_w refers to density of water, α, m, n are parameters of the van Genuchten model, m=1-1/n, and m=1-2/n.

2.3.2 Generalized VG SFCC model

Wen et al. (2020) indicated that θ at 0 °C determined by Eq. 1 was equal to θ_s, which was not suitable for the unsaturated soil samples. Hence, θ_s was replaced by initial volumetric water content, and a generalized VG SFCC (GVG SFCC) model was obtained.

$$\theta = \theta_r + (\theta_0 - \theta_r)\left[\frac{1}{1+\left(-\frac{\alpha L \rho_w}{273.15}T\right)^n}\right]^m \quad (2)$$

where θ_0 refers to initial volumetric water content.

2.3.3 A new SFCC model containing freezing/thawing point

Freezing/thawing point represents the boundary between unfrozen and frozen states (Wang et al., 2018). The SFCC remains unchanged when temperature is larger than freezing/thawing point (Wang et al., 2017; Zhang et al., 2018; Li et al., 2020). Previous studies seldom considered the freezing/thawing

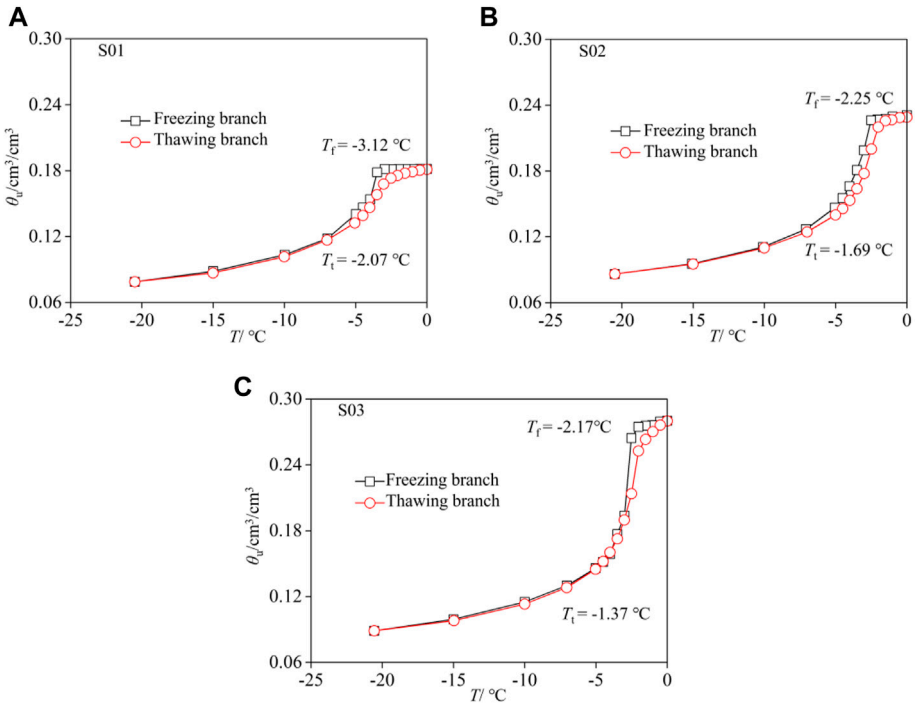

FIGURE 3
Effect of initial water content on the SFCC.

point in the model, which may lead to a biased unfrozen water content at freezing/thawing point and 0°C. Therefore, a new equation containing the freezing/thawing point was developed, as shown in Eq. 3.

$$\theta = \begin{cases} \theta_r + (\theta_0 - \theta_r)\left[\dfrac{1}{1+\left(\frac{T}{T_{f/t}}-1\right)^n}\right]^m & T < T_{f/t} \\ \theta_0 & T \geq T_{f/t} \end{cases} \quad (3)$$

where $T_{f/t}$ is the freezing/thawing point, and m=1-1/n.

3 Results and discussion

3.1 Effect of soil properties on the SFCC

3.1.1 Effect of initial water content

Figure 3 shows the results of three soil samples with three initial gravimetric water contents (11% for S01, 14% for S02, 17% for S03) and same dry density (1.65 g/cm^3). The freezing points (T_f) for S01, S02 and S03 were -3.12°C, -2.25°C and -2.17°C, respectively, while the thawing points (T_t) for S01, S02 and S03 were -2.07°C, -1.69°C and -1.37°C, respectively. It can be concluded that increasing initial water content leads to the increase of T_f (T_t). It can be explained by the Gibbs-Thomson equation and bundle of cylindrical capillary model (Zhou et al., 2015). A larger initial water content leads to a larger cylindrical capillary. Based on the Gibbs-Thomson equation, a larger cylindrical capillary indicates a larger freezing point.

The SFCC during a freezing-thawing process can be categorized into three stages (Zhang et al., 2018). In the freezing process, SFCC seldom changes in the temperature range of T_f to 0°C (Stage 1). Once the temperature drops below T_f, the SFCC sharply decreases and a large quantity of ice forms (Stage 2). At a certain subzero temperature, further decreasing temperature does not significantly reduce the unfrozen water (Stage 3). The similar trend can be also observed in the thawing process. At a subzero temperature, the unfrozen water content in freezing branch of SFCC was larger than that in the thawing branch of SFCC, owing to the freezing-thawing hysteresis effect (Tian et al., 2014). The hysteresis effect was obvious in the higher temperature range (-5°C to 0). When the temperature was below -10°C, the thawing branch of SFCC was almost the same as the freezing branch, indicating that the hysteresis behavior was not obvious in this temperature range. The same results have been reported by Li et al. (2020).

3.1.2 Effect of dry density

Figure 4 shows the SFCC of two soil samples with two dry densities (1.65 g/cm^3 for S02 and 1.55 g/cm^3 for S04) and same

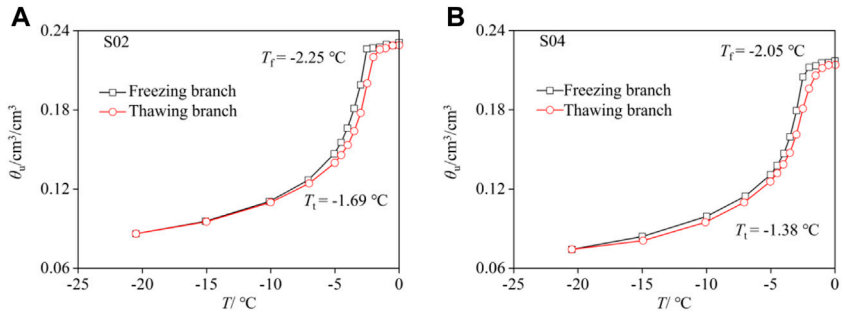

FIGURE 4
Effect of dry density on the SFCC.

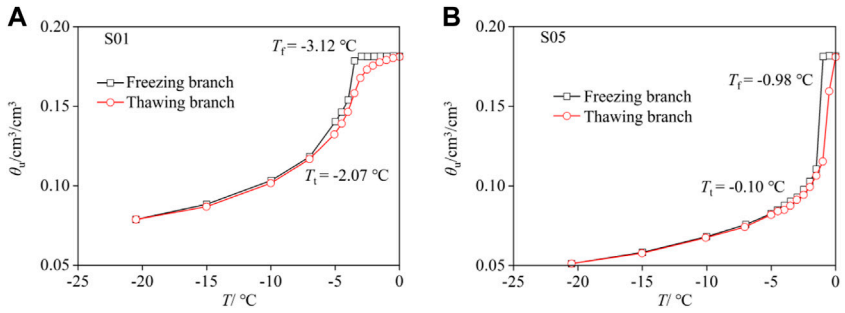

FIGURE 5
Effect of soil type on the SFCC.

gravimetric water content (14%). T_f values for S02 and S04 were -2.25°C and -2.05°C, respectively, while T_t values for S02 and S04 were -1.69°C and -1.38°C, respectively. A small increase in the T_f and T_t was observed between S02 and S04. It can be attributed to the small decrease in dry density (i.e., 6.45% decrease in dry density between S02 and S04). With the decrease of dry density, the amount of large pores decreases significantly and the amount of small pores seldom changes. The large pore change affects the T_f and T_t. The changing trend and slope of two SFCCs with different dry densities were similar. Both soil samples exhibited hysteresis behavior. Compared to the lower temperature range (<-10°C), the hysteresis behavior was more obvious in the higher temperature range (-5°C < T < 0). The SFCC at the lowest measured subzero temperature was different. Volumetric unfrozen water at the lowest measured subzero temperature gradually increased with the increase of dry density.

3.1.3 Effect of soil type

Figure 5 shows the SFCC of two different soils. S01 was loess sample, while S05 was loess-sand mixture. T_f values for S01 and S05 were -3.12°C and -0.98°C, respectively, while T_t values for S01 and S05 were -2.07°C and -0.10°C, respectively. It indicated that soil type had a great influence on T_f and T_t. For S05, the SFCC started to decrease at -0.98°C. In contrast, the SFCC of S01 was relatively flat and seldom changed in the temperature range of -3.12°C–0°C. In stage 2, the SFCC sharply decreased with the decrease of subzero temperature. The slope of SFCC was steep for S05, while the slope of SFCC for S01 was gentle. This indicated that the unfrozen water in S05 dropped at a faster rate than that in S01. The unfrozen water content at the lowest measured subzero temperature of S05 is smaller than that of S01. These may be because S01 can store more unfrozen water by larger adsorptive forces owing to its larger specific surface area and higher fine content (Ren and Vanapalli, 2018). The loess-sand mixture also exhibited hysteresis behavior, but it was obvious in a narrower temperature range compared to S01.

3.1.4 Effect of desalination

Figure 6 investigates the effect of desalination on the SFCC. S01 was loess sample, while S06 was desalted loess sample. The

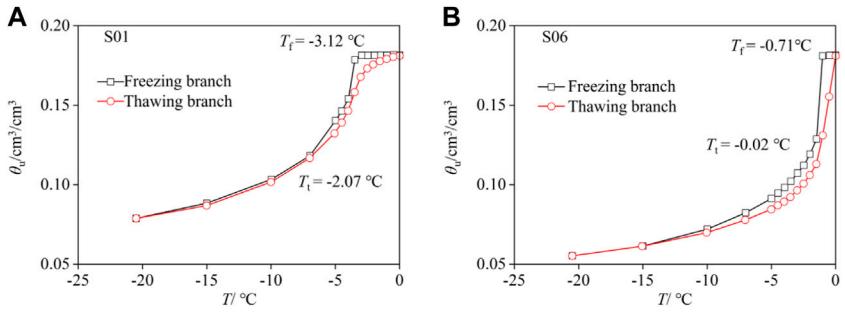

FIGURE 6
Effect of desalination on the SFCC.

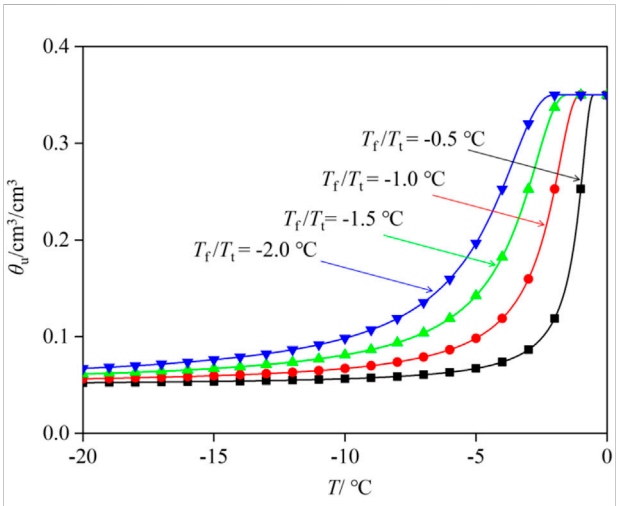

FIGURE 7
Effect of the parameter T_f/T_t on the new model.

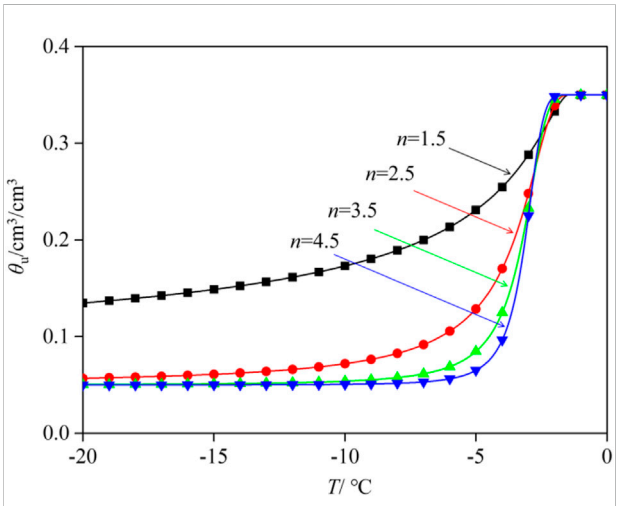

FIGURE 8
Effect of the parameter n on the new model.

two soil samples had same initial gravimetric water content (11%) and dry density (1.65 g/cm^3). T_f values for S01 and S05 were -3.12°C and -0.71°C, respectively, while T_t values for S01 and S05 were -2.07°C and -0.02°C, respectively. Desalination greatly affected the SFCC. For the desalted loess sample (S06), the SFCC significantly decreased at -0.71 °C. However, the SFCC of loess sample (S01) seldom changed in the temperature range of -3.12°C–0°C. The significant differences of SFCC between S01 and S06 may be due to the larger amount of fine and salt contents of S01 compared to S06. Xu et al. (2016) investigated the grain size distributions of a soil and a desalted soil, and indicated that the quantity of solid particles smaller than 0.075 mm in the desalted soil was lower than that in the natural soils. For S06, the salt and fine contents may be lost during the desalting process, resulting in a weakened ability to retain unfrozen water by adsorptive forces (Xu et al., 2016; Xu et al., 2017).

3.2 General features of the new model

Figure 7 shows the effect of parameter T_f/T_t on the SFCC when n=2.3, θ_r=0.05, θ_0=0.35, and T_f/T_t decreases from -0.5°C to -2.0°C. When the temperature is larger than T_f/T_t, the SFCC remains unchanged during the freezing/thawing process. When the temperature is lower than T_f/T_t, the SFCC with a larger value of T_f/T_t declines at a faster rate than that with a lower value of T_f/T_t, and the shape and slope of SFCC change with temperature.

Figure 8 indicates the effect of parameter n on the SFCC when T_f/T_t=-1.5°C, θ_r=0.05, θ_0=0.35, and n increases from 1.5 to 4.5. The parameter n significantly affects the slope of the SFCC during the freezing/thawing process. The SFCC with a smaller value of n resembles the letter "S" with a gentler slope, while the SFCC with a larger value of n resembles the letter "S" with a steeper slope. Parameter n also reflects the ability to retain

unfrozen water. For a larger value of n, unfrozen water significantly reduces with the decrease of temperature.

3.3 Model valuation and comparisons

The current experimental data were applied to evaluated the performance of the proposed model and four other models (GVG SFCC model with m=1-1/n, GVG SFCC model with m=1-2/n, VG SFCC model with m=1-1/n, and VG SFCC model with m=1-2/n). Figure 9 indicated that the new model performed best among the five models for all the six soil samples. The new model accurately captured the variation of SFCC during a freezing-thawing process. In the temperature range of T_f/T_t to 0°C, the SFCC calculated by the new model remained unchanged with the decrease of temperature and matched well with the experimental results. Further decreasing temperature led to a continuously decrease of SFCC with temperature. The GVG SFCC model with m=1-1/n and GVG SFCC model with m=1-2/n had similar trends, but the GVG SFCC model with m=1-2/n performed better than the GVG SFCC model with m=1-1/n, especially in the temperature range of -10 to -2 °C.

Figure 9 showed that the SFCCs determined by the VG SFCC model with m=1-1/n and VG SFCC model with m=1-2/n usually had computational oddity in the temperature range of T_f to 0°C. For example, the two models significantly overestimated the unfrozen water content near 0°C. It can be attributed to the fact that the calculated volumetric unfrozen water content determined by the VG SFCC model with m=1-1/n and VG SFCC model with m=1-2/n at 0°C was equal to saturated volumetric unfrozen water content, and the measured value was the initial volumetric unfrozen water content. The significant difference between measured and calculated results at 0°C led to the biased SFCC determined by the two models. In the lower temperature range, the two models overestimated the SFCC.

Figure 10 shows the comparison of the calculated and measured SFCC with 1:1 line for the five models. Similar to the above analysis, the new model performed best among the five models. The GVG SFCC model with m=1-1/n and GVG SFCC model with m=1-2/n also performed very well, and all the data points clustered around 1:1 line. For the VG SFCC model with m=1-1/n and VG SFCC model with m=1-2/n, the two models performed well when the volumetric unfrozen water content was lower than 0.2 cm^3/cm^3, and obtained unsatisfactory results when the volumetric unfrozen water content was larger than 0.2 cm^3/cm^3. It can be attributed to the fact that the saturated volumetric unfrozen water content was included in the two models.

The performance of the models was evaluated with root mean squared error (*RMSE*) and average deviations (*AD*). Table 3 shows that the new model has the lowest value of *RMSE* in different branches (freezing branch, thawing branch and both branches),

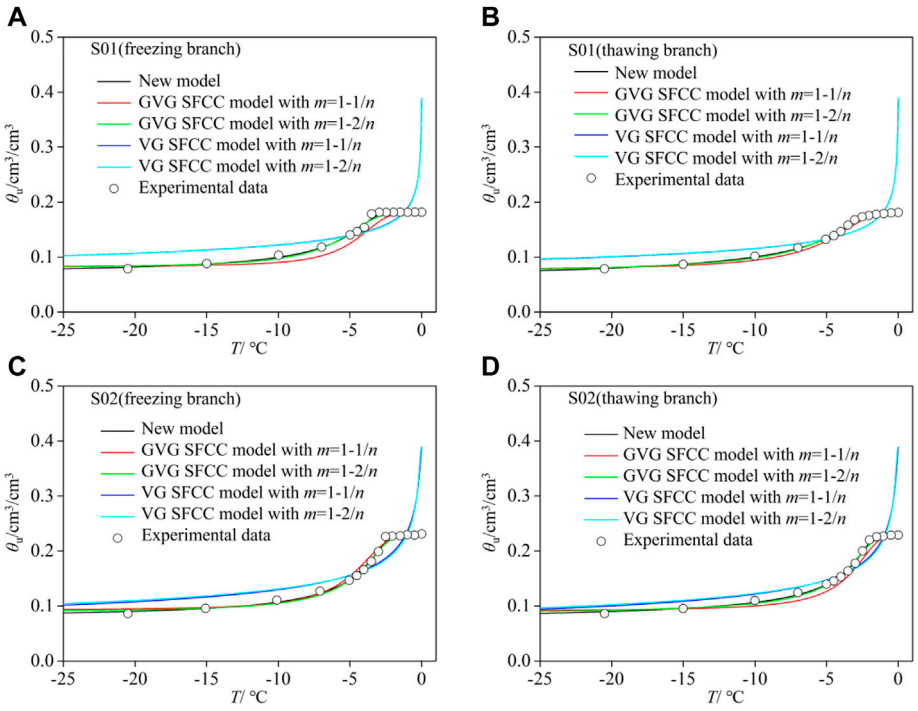

FIGURE 9
(Continued).

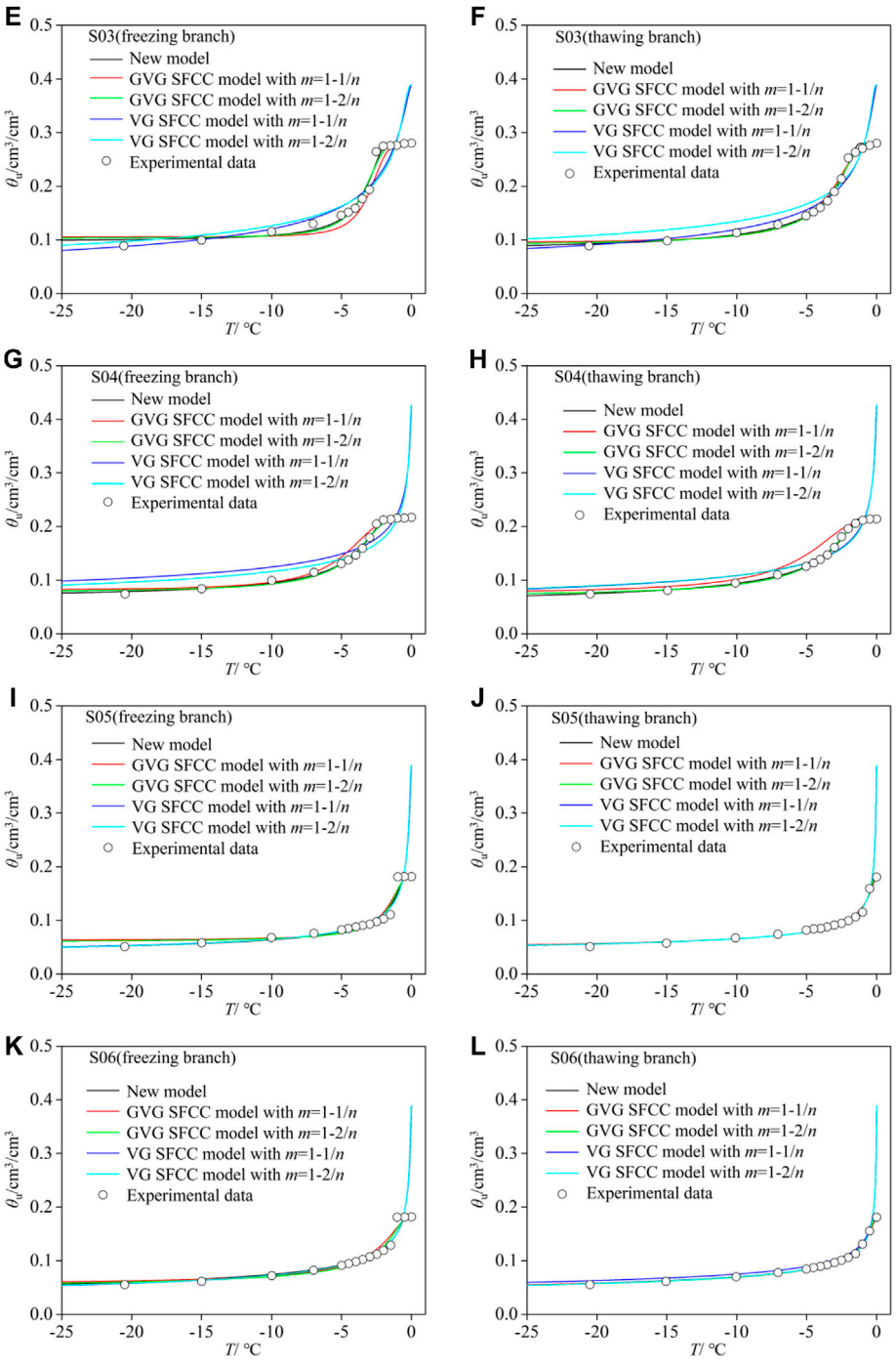

FIGURE 9
(Continued). Comparison of measured SFCC (symbols) and estimated SFCC (lines) as a function of temperature

suggesting that the new model performed best among the five models, followed by the GVG SFCC model with m=1-2/n, GVG SFCC model with m=1-1/n, VG SFCC model with m=1-1/n, and VG SFCC model with m=1-2/n. Compared to the freezing branch, the SFCC model performed better in the thawing branch. From Table 4, the positive AD values revealed that the new model, VG SFCC model with m=1-1/n, and VG SFCC model with m=1-2/n usually overestimated the SFCC, and the negative AD values

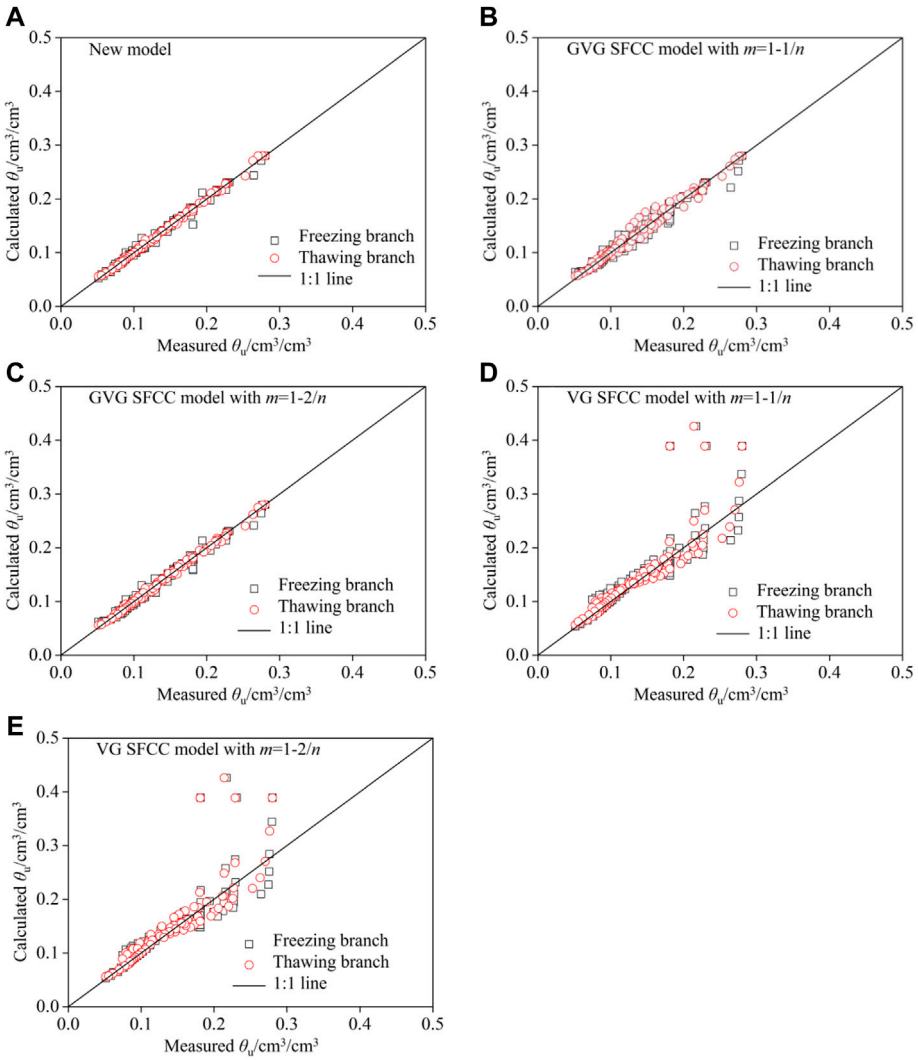

FIGURE 10
Comparison of measured and estimated SFCC.

TABLE 3 *RMSE* for different SFCC models.

Branch	New model	GVG SFCC model		VG SFCC model	
	m=1-1/*n*	*m*=1-1/*n*	*m*=1-2/*n*	*m*=1-1/*n*	*m*=1-2/*n*
Freezing branch	0.0067	0.0111	0.0074	0.0518	0.0520
Thawing branch	0.0029	0.0085	0.0034	0.0504	0.0508
Both branches	0.0052	0.0099	0.0058	0.0511	0.0514

indicated that the GVG SFCC model with *m*=1-2/*n* usually underestimated the SFCC. The GVG SFCC model with *m*=1-1/*n* underestimated the SFCC in the freezing branch and overestimated the SFCC in the thawing branch. Based on the above analysis, it can be concluded that the new SFCC model accurately mimicked the variations of SFCC during a freezing-thawing process.

TABLE 4 *AD* for different SFCC models.

Branch	New model	GVG SFCC model		VG SFCC model	
	m=1-1/n	m=1-1/n	m=1-2/n	m=1-1/n	m=1-2/n
Freezing branch	0.0001	-0.0011	-0.0006	0.0147	0.0132
Thawing branch	0.0004	0.0005	-0.0001	0.0140	0.0143
Both branches	0.0002	-0.0003	-0.0003	0.0144	0.0137

TABLE 5 Boundary conditions for different SFCC models.

Models	T=T_f/T_t	T=0 °C
New model (m=1-1/n)	θ_0	θ_0
GVG SFCC model (m=1-1/n)	$\theta_r + (\theta_0 - \theta_r)[\frac{1}{1+(-\frac{\alpha L \rho_w}{273.15} T_{f/t})^n}]^{1-1/n}$	θ_0
GVG SFCC model (m=1-2/n)	$\theta_r + (\theta_0 - \theta_r)[\frac{1}{1+(-\frac{\alpha L \rho_w}{273.15} T_{f/t})^n}]^{1-2/n}$	θ_0
VG SFCC model (m=1-1/n)	$\theta_r + (\theta_s - \theta_r)[\frac{1}{1+(-\frac{\alpha L \rho_w}{273.15} T_{f/t})^n}]^{1-1/n}$	θ_s
VG SFCC model (m=1-2/n)	$\theta_r + (\theta_s - \theta_r)[\frac{1}{1+(-\frac{\alpha L \rho_w}{273.15} T_{f/t})^n}]^{1-2/n}$	θ_s

3.4 Strengths and limitations of the proposed model

Previous researches have indicated that unfrozen water content remained unchanged in the temperature range of T_f/T_t to 0 °C (Zhang et al., 2018; Kong et al., 2020). Two different temperatures (T_f/T_t and 0 °C) were applied to study the boundary conditions of different models. Table 5 summarized the unfrozen water contents at two temperatures. It showed that the unfrozen water contents at T_f/T_t varied significantly. The unfrozen water content determined by the new model was equal to θ_0, which satisfied the theoretical analysis (Zhang et al., 2018; Kong et al., 2020). However, for the other four SFCC models, the unfrozen water contents at T_f/T_t were smaller than θ_0 and varied significantly. When T=0 °C, the calculated results should be θ_0. However, the results determined by VG SFCC model with m=1-1/n and VG SFCC model with m=1-2/n were θ_s, which disagreed with the theoretical analysis (Zhang et al., 2018; Kong et al., 2020). The new model satisfied the theoretical analysis at T_f/T_t and 0°C. Therefore, we can conclude that the new model is best among the five SFCC models.

The proposed SFCC model contains an independent variable (subzero temperature), which is simple and easy to use. The lowest value of RMSE indicates that the new model has good fitting performance. However, the new model cannot be used to estimate SFCC using some easy-to-obtain soil parameters. Further studies should attempt to develop a relationship between the parameter n and soil parameters (e.g. initial water content, dry density, liquid limit, plastic limit, plasticity index, specific surface area), which will benefit for the numerical modelling in cold regions.

4 Conclusion

This study investigated the effects of initial water content, dry density, soil type, and desalination on the SFCC during a freezing-thawing process. A new equation of SFCC containing a freezing/thawing point was proposed. The current experimental results were applied to evaluate the performance of the new models and four other models. The following conclusions can be drawn:

(1) The initial water content, soil type and desalination have a large effect on the SFCC, while the dry density has an insignificant effect on the SFCC.
(2) Hysteresis behavior can be observed from the SFCCs of freezing branch and thawing branch. Hysteresis behavior is obvious in the higher temperature range (-5°C < T < 0), but not in the lower temperature range (T ≤ -10°C).
(3) The new model accurately calculated the SFCC during a freezing-thawing process, especially in the higher temperature range. In addition, it has simple formula and is continuous near freezing/thawing point and 0°C, which can be easily incorporating into the numerical algorithms for coupled heat and mass transfer in cold regions.

Data availability statement

The raw data supporting the conclusion of this article will be made available by the authors, without undue reservation.

Author contributions

JB: Conceptualization, Methodology, Writing—Original draft, ZW: Conceptualization, Supervision, Funding acquisition, Writing—Review and Editing, YL: Investigation, Writing—Review and Editing, HW: Writing—Review and Editing, YZ: Investigation, Writing—Review and Editing, YS:

Investigation, Writing—Review and Editing, TW: Investigation, GW: Investigation, Software.

Funding

This study was financially supported by the National Natural Science Foundation of China (Grant No. 42102306), the Second Tibetan Plateau Scientific Expedition and Research (STEP) Program (Grant No. 2019QZKK0905), the National Earthquake Science Joint Foundation of China (Grant No. U1939209), the program of the State Key Laboratory of Road Engineering Safety and Health in Cold and High-Altitude Regions (Grant No. YGY2020KYPT-07), the Open Fund of State Key Laboratory of Frozen Soil Engineering (Grant No. SKLFSE202108, SKLFSE202009), and the Project of the State Key Laboratory of Frozen Soil Engineering (Grant No. SKLFSE-ZQ-57).

Conflict of interest

YZ was employed by the CCCC First Harbor Consultants Co., Ltd.

The remaining authors declare that the research was conducted in the absence of any commercial or financial relationships that could be construed as a potential conflict of interest.

Publisher's note

References

Bi, J., Chen, W., Zhang, J., Zhang, Y., Fan, W., and Jia, B. (2019). A modified calculation model for the saturation-dependent thermal conductivity of fine-textured soils. *Results Phys* 15, 102673. doi:10.1016/j.rinp.2019.102673

Bi, J., Zhang, M., Lai, Y., Pei, W., Lu, J., You, Z., et al. (2020). A generalized model for calculating the thermal conductivity of freezing soils based on soil components and frost heave. *Int. J. Heat Mass Transf.* 150, 119166. doi:10.1016/j.ijheatmasstransfer.2019.119166

Bittelli, M., Flury, M., and Campbell, G. S. (2003). A thermodielectric analyzer to measure the freezing and moisture characteristic of porous media. *Water Resour. Res.* 39. doi:10.1029/2001WR000930

Kong, L., Wang, Y., Sun, W., and Qi, J. (2020). Influence of plasticity on unfrozen water content of frozen soils as determined by nuclear magnetic resonance. *Cold Regions Sci. Technol.* 172, 102993. doi:10.1016/j.coldregions.2020.102993

Konrad, J. M. (1994). Sixteenth Canadian geotechnical colloquium: Frost heave in soils: Concepts and engineering. *Can. Geotech. J.* 31, 223–245. doi:10.1139/t94-028

Kozlowski, T., and Nartowska, E. (2013). Unfrozen water content in representative bentonites of different origin subjected to cyclic freezing and thawing. *Vadose Zone J.* 12, vzj2012.0057. doi:10.2136/vzj2012.0057

Li, Z., Chen, J., and Sugimoto, M. (2020) Pulsed NMR measurements of unfrozen water content in partially frozen soil. *J. Cold Reg. Eng.* 34:04020013. doi:10.1061/(ASCE)CR.1943-5495.0000220

Liu, J., Yang, P., and Yang, Z. (2020). Electrical properties of frozen saline clay and their relationship with unfrozen water content. *Cold Regions Sci. Technol.* 178, 103127. doi:10.1016/j.coldregions.2020.103127

Ming, F., Pei, W., Zhang, M., and Chen, L. (2022). A hydraulic conductivity model of frozen soils with the consideration of water films. *Eur. J. Soil Sci.* 73, e13210. doi:10.1111/ejss.13210

Mu, Q. Y., Zhou, C., Ng, C. W. W., and Zhou, G. G. D. (2019). Stress effects on soil freezing characteristic curve: Equipment development and experimental results. *Vadose zone J.* 18, 1–10. doi:10.2136/vzj2018.11.0199

Nishimura, S., Gens, A., Olivella, S., and Jardine, R. J. (2009). THM-Coupled finite element analysis of frozen soil: Formulation and application. *Géotechnique* 59, 159–171. doi:10.1680/geot.2009.59.3.159

Patterson, D. E., and Smith, M. W. (1985). Unfrozen water content in saline soils: Results using time-domain reflectometry. *Can. Geotech. J.* 22, 95–101. doi:10.1139/t85-009

Ren, J., Vanapalli, S. K., and Han, Z. (2017). Soil freezing process and different expressions for the soil-freezing characteristic curve. *Sci. Cold Arid Regions* 9, 221–228. doi:10.3724/SP.J.1226.2017.00221

Ren, J., and Vanapalli, S. K. (2018). Prediction of resilient modulus of frozen unbound road materials using soil-freezing characteristic curve. *Can. Geotech. J.* 55, 1200–1207. doi:10.1139/cgj-2017-0153

Tian, H., Wei, C., Wei, H., and Zhou, J. (2014). Freezing and thawing characteristics of frozen soils: Bound water content and hysteresis phenomenon. *Cold Regions Sci. Technol.* 103, 74–81. doi:10.1016/j.coldregions.2014.03.007

Wang, C., Lai, Y., Yu, F., and Li, S. (2018). Estimating the freezing-thawing hysteresis of chloride saline soils based on the phase transition theory. *Appl. Therm. Eng.* 135, 22–33. doi:10.1016/j.applthermaleng.2018.02.039

Wang, C., Lai, Y., and Zhang, M. (2017). Estimating soil freezing characteristic curve based on pore-size distribution. *Appl. Therm. Eng.* 124, 1049–1060. doi:10.1016/j.applthermaleng.2017.06.006

Watanabe, K., and Wake, T. (2009). Measurement of unfrozen water content and relative permittivity of frozen unsaturated soil using NMR and TDR. *Cold Regions Sci. Technol.* 59, 34–41. doi:10.1016/j.coldregions.2009.05.011

Wen, H., Bi, J., and Guo, D. (2020). Evaluation of the calculated unfrozen water contents determined by different measured subzero temperature ranges. *Cold Regions Sci. Technol.* 170, 102927. doi:10.1016/j.coldregions.2019.102927

Wen, Z., Ma, W., Feng, W., Deng, Y., Wang, D., Fan, Z., et al. (2012). Experimental study on unfrozen water content and soil matric potential of Qinghai-Tibetan silty clay. *Environ. Earth Sci.* 66, 1467–1476. doi:10.1007/s12665-011-1386-0

Xiao, Z., Lai, Y., and Zhang, J. (2020). A thermodynamic model for calculating the unfrozen water content of frozen soil. *Cold Regions Sci. Technol.* 172, 103011. doi:10.1016/j.coldregions.2020.103011

Xiao, Z., Lai, Y., and Zhang, M. (2018). Study on the freezing temperature of saline soil. *Acta Geotech.* 13, 195–205. doi:10.1007/s11440-017-0537-1

Xu, X., Wang, Y., Bai, R., Fan, C., and Hua, S. (2016). Comparative studies on mechanical behavior of frozen natural saline silty sand and frozen desalted silty sand. *Cold Regions Sci. Technol.* 132, 81–88. doi:10.1016/j.coldregions.2016.09.015

Xu, X., Wang, Y., Yin, Z., and Zhang, H. (2017). Effect of temperature and strain rate on mechanical characteristics and constitutive model of frozen Helin loess. *Cold Regions Sci. Technol.* 136, 44–51. doi:10.1016/j.coldregions.2017.01.010

You, Z., Lai, Y., Zhang, M., and Liu, E. (2017). Quantitative analysis for the effect of microstructure on the mechanical strength of frozen silty clay with different contents of sodium sulfate. *Environ. Earth Sci.* 76, 143. doi:10.1007/s12665-017-6454-7

Zhang, M., Zhang, X., Lu, J., Pei, W., and Wang, C. (2018). Analysis of volumetric unfrozen water contents in freezing soils. *Exp. Heat. Transf.* 32, 426–438. doi:10.1080/08916152.2018.1535528

Zhang, S., Teng, J., He, Z., and Sheng, D. (2016). Importance of vapor flow in unsaturated freezing soil: A numerical study. *Cold Regions Sci. Technol.* 126, 1–9. doi:10.1016/j.coldregions.2016.02.011

Zhou, J., Tan, L., Wei, C., and Wei, H. (2015). Experimental research on freezing temperature and super-cooling temperature of soil. *Rock Soil Mech.* 36 (3), 777–785. doi:10.16285/j.rsm.2015.03.023

Appendix A

The mass of the over-dried loess, over-dried sand and distilled deionized water for one sample can be determined by Eqs. (A.1)-(A.3).

$$m_{\text{loess}} = C_{\text{loess}}\rho_{\text{d}}V \tag{A.1}$$

$$m_{\text{sand}} = C_{\text{sand}}\rho_{\text{d}}V \tag{A.2}$$

$$m_{\text{water}} = (w_{\text{d}} - w_{\text{o}})\rho_{\text{d}}V \tag{A.3}$$

where m_{loess} is the mass of over-dried loess in one specimen; m_{sand} is the mass of over-dried sand in one specimen; m_{water} is the mass of water in one specimen; V is the volume of one specimen; C_{loess} is the loess content of one specimen, %; C_{sand} is the sand content of one specimen, %; C_{loess}+C_{sand} =100%; w_{d} is the desired water content of one specimen, %; w_{o} is the initial water content of over-dried soil sample, %, w_{o}=0.

Appendix B

By substituting the Clapeyron equation (Eq. (B.1)) into VG SWCC model (Eq. (B.2)), the VG SFCC model (Eq. 1) can be obtained (Ren et al., 2017; Wen et al., 2020; Zhang et al., 2016).

$$\psi_{\text{cryo}} = -L\rho_{\text{w}}\ln\frac{T + 273.15}{273.15} \approx -L\rho_{\text{w}}\frac{T}{273.15} \tag{B.1}$$

$$S_{\text{e}} = \frac{\theta - \theta_{\text{r}}}{\theta_{\text{s}} - \theta_{\text{r}}} = \left[\frac{1}{1 + (\alpha\psi)^{n}}\right]^{m} \tag{B.2}$$

where ψ_{cryo} refers to cryogenic suction, and S_{e} refers to effective saturation.